Langmuir

Article

pubs.acs.org/Langmuir

Variation of Formal Hydrogen-Bonding Networks within Electronically Delocalized π-Conjugated Oligopeptide Nanostructures

Brian D. Wall,[†] Yuecheng Zhou,[∥] Shao Mei,[∥] Herdeline Ann M. Ardoña,[†,‡] Andrew L. Ferguson,[∥] and John D. Tovar*[,†,‡,§]

[†]Department of Chemistry, Krieger School of Arts and Sciences, [‡]Institute of NanoBioTechnology, and [§]Department of Materials Science and Engineering, Whiting School of Engineering, Johns Hopkins University, 3400 N. Charles St., Baltimore, Maryland 21218, United States

[∥]Department of Materials Science and Engineering, University of Illinois at Urbana−Champaign, Urbana, Illinois 61801, United States

Supporting Information

ABSTRACT: This photophysical study characterizes the generality of intermolecular electronic interactions present within nanomaterials derived from self-assembling oligopeptides with embedded π-conjugated oligophenylenevinylene (OPV) subunits stilbene and distyrylbenzene that in principle present two distinct β-sheet motifs. Two different synthetic approaches led to oligopeptides that upon self-assembly are expected to self-assemble into multimeric aggregates stabilized by β-sheet-like secondary structures. The target molecules express either two C-termini linked to the central OPV core (symmetric peptides) or the more common N-termini to C-termini polarity typical of natural oligopeptides (nonsymmetric peptides). Both peptide secondary structures were shown to form extended 1-D peptide aggregates with intimate intermolecular π-electron interactions. Differences in length of the π-conjugated OPV segments resulted in differing extents of intermolecular interactions and the resulting photophysics. The peptides containing the shorter stilbene (OPV2) units showed little ground state interactions and resulted in excimeric emission, while the longer distyrylbenzene (OPV3) peptides had different ground state interactions between adjacent π-conjugated subunits resulting in either perturbed electronic properties arising from exciton coupling or excimer-like excited states. Molecular dynamics simulations of nascent aggregate formation predict peptide dimerization to be a spontaneous process, possessing thermodynamic driving potentials in the range 2−6 kcal/mol for the four molecules considered. Antiparallel stacking of the peptides containing an OPV3 subunit is thermodynamically favored over the parallel orientation, whereas both arrangements are equally favored for the peptides containing an OPV2 subunit. This study validates the generality of peptide-π-peptide self-assembly to provide electronically delocalized supramolecular structures and suggests flexibility in peptide sequence design as a way to tune the material properties of π-conjugated supramolecular polymers.

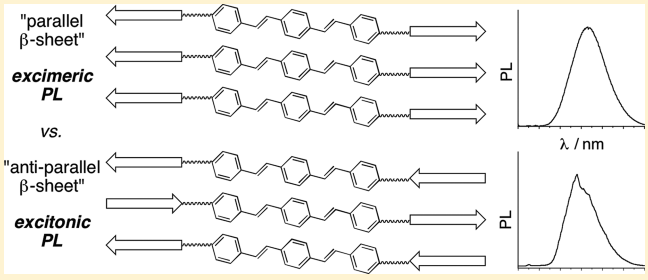

INTRODUCTION

The folding and assembly of natural biological proteins underpin many biological processes essential to life. Synthetic oligopeptides have demonstrated great potential to self-assemble unique macromolecular architectures with desirable structural and functional properties.[1] The rich structural possibilities when considering differing levels of peptide organization, from primary amino acid sequence to secondary and tertiary structure, showcase the power of peptides as versatile scaffolds for materials development. Beyond their structural diversity, the ability for peptides to assemble under biologically relevant conditions and have specific interactions with biological systems create a niche for powerful biomaterials and tissue engineering schemes.[2] The ability to control the macromolecular architecture of peptide-based materials opens up possibilities to rationally engineer the resulting materials at the molecular level.[3,4] The overall properties of a peptidic material can be tuned through variation in primary amino acid sequence and biological functionality can even be directly perturbed by the peptidic with which it associates.[5]

The intermolecular associations among oligopeptides in their assembled states can also be used in conjunction with π-conjugated systems to drastically alter their (opto)electronic properties.[6−10] Such modifications in principle should lead to an aggressive perturbation of protein-based assembly especially when non-natural aromatic quadrupoles of π-conjugated subunits are incorporated directly into the peptide backbones. However, recent work from several laboratories has validated

Received: May 22, 2014
Revised: July 21, 2014
Published: September 2, 2014

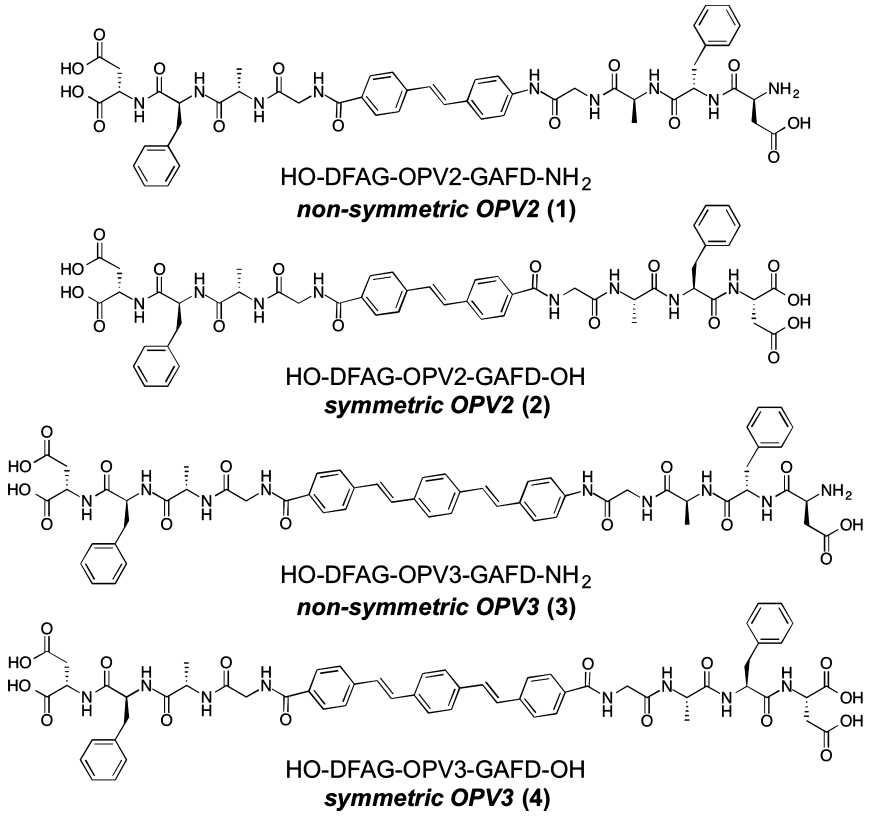

Figure 1. DFAG peptides with different N-to-C backbone directionalities and different OPV lengths.

the self-assembly paradigm for peptide-π-peptide triblock molecules where the π-conjugated internal units provide spectroscopic handles for investigating peptide self-assembly.[11−14] The abilities to influence peptide association in a predictable way and tune the intended macromolecular structures are crucial. In this report we describe how the nature of the peptide-based hydrogen-bonding network influences the self-assembly and the nanostructural electronic properties. Non-natural oligopeptides with the ability to form 1-D supramolecular aggregates with differing hydrogen bonding motifs offer new design opportunities for unique electronic biomaterials. The goal of this study is to provide new electronic information about how the differences of peptide aggregation as a primary function of hydrogen bonding motif can influence optoelectronic properties of peptide aggregates. In a more general sense, these studies also provide governing principles to rationally design specific types of supramolecular aggregates that may be useful in the development of biologically relevant optoelectronic biomaterials.

RESULTS AND DISCUSSION

We designed and synthesized four oligopeptides with embedded phenylenevinylene chromophores as shown in Figure 1 and studied their photophysical and morphological properties. The oligopeptides studied here all consisted of the same primary amino acid sequence, DFAG, with respect to residue placement relative to the central π-conjugated core, although the peptide backbone directionalities differ for each of the two chromophore examples (Figure 1). The tetrapeptide DFAG was chosen to provide adequate aqueous solubility at neutral or basic pH and to undergo self-assembly upon lowering the pH due to formal protonation of the carboxylate side chains. We chose the oligophenylenevinylene chromophores (OPVs) due to their established photophysical properties, including stilbene (OPV2) and distyrylbenzene (OPV3). In one presentation, the same sense of the peptide N-to-C linkages (or "directionality") was maintained along the length of the molecule, thus leading to a final molecule with one distinct N- and C-terminus (referred to here as "nonsymmetric") while in another presentation, the N-to-C directionality emanates in opposing directions from the central π-conjugated core in a mirror image sense, thus leading to a final molecule presenting two C-termini (referred to here as "symmetric"). We synthesized peptide-based OPV materials with these two differing peptide sequence presentations using methods developed in our lab as described further below. We previously demonstrated how the variation of the peptide sequence peripheral to the central chromophore unit impacts the photophysical properties of the resulting supramolecular nanostructures,[15] and in this case we are in essence maintaining the same structural units albeit with different backbone directionality. In this report, we examine how these peptide N-to-C polarities influence nanostructure photophysics, using well-studied OPVs as prototypical examples.

Synthesis of OPV Amidation Partners and Peptides. We reported several synthetic approaches to peptide-based organic electronic materials, and we employ two of these approaches here. The first method (leading to nonsymmetric peptides **1** and **3**) utilized π-conjugated OPV "amino acids" as functional mimics of standard α-amino acids compatible with standard solid-phase peptide synthesis (SPPS),[11] where the activated acid moiety of the amino acid N-acylated the amine terminus of the growing oligopeptide while at the same time presented a new (but protected) amine functionality for continued amide bond formation. This synthesis approach

dx.doi.org/10.1021/la501999g | Langmuir 2014, 30, 11375−11385

maintained the same sense of the peptide N-to-C linkages along the length of the molecule. The second method (leading to symmetric peptides **2** and **4**) used π-conjugated diacids in an on-resin site−site dimerization procedure that links two peptide amine termini via amidation/N-acylation onto a common π-electron core.[16] Using the amino acid and diacid π-systems for oligopeptide synthesis, we can now synthesize self-assembling oligopeptide-π OPV hybrid models with different peptide polarity presentation to probe how this important macromolecular assembly variable specifically impacts nanostructural and electronic properties. We discuss briefly the synthesis of the individual amino acid or diacid amidation partners used for the peptide synthesis. More specific details regarding the peptide syntheses can be found in the Supporting Information.

The OPV2 amino acid was synthesized through a Horner−Wadsworth−Emmons olefination with diethyl 4-nitrobenzylphosphonate[17] and methyl 4-formylbenzoate (Figure 2a).[18]

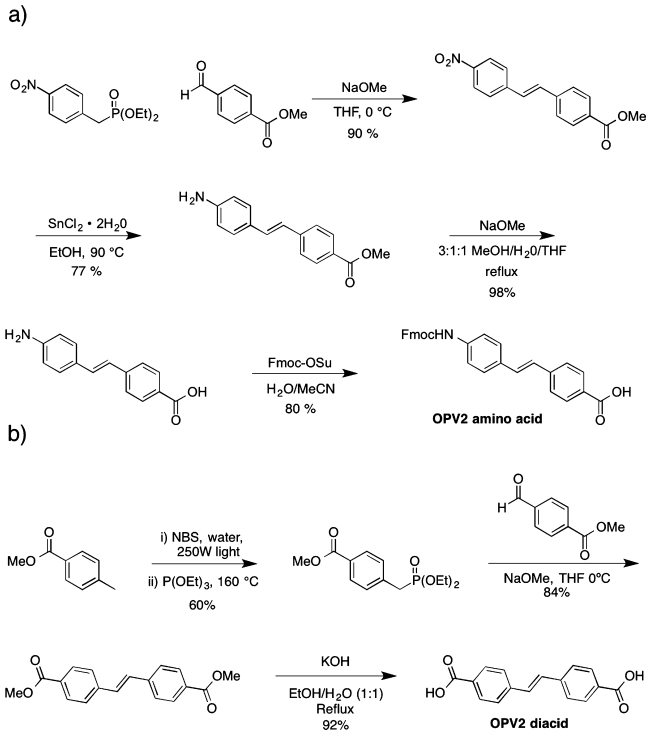

Figure 2. Synthesis of OPV2 amino acid (a) and diacid (b) for incorporation into nonsymmetric and symmetric peptide backbones present in **1** and **2**, respectively.

Reduction of the nitro group using stannous chloride followed by ester saponification and Fmoc protection of the amine gave the OPV2 amino acid that could be used directly with SPPS. Amidation between the OPV2 amino acid and the N-deprotected peptide resin took place under normal HBTU activation conditions. After Fmoc deprotection of the resin bound OPV2, the weaker nucleophilicity of the resulting aryl amine required the use of more electrophilic coupling reagents for the next step in the SPPS sequence. The coupling of the next amino acid was completed with the use of triphosgene and 2,6-lutidine,[19] and all couplings of the remaining amino acids could be completed using standard activation procedures ultimately yielding nonsymmetric OPV2 (**1**). The OPV2 diacid was synthesized through a Horner−Wadsworth−Emmons olefination between diethyl 4-(methoxycarbonyl)-benzylphosphonate[18] and methyl 4-formylbenzoate to give the stilbene dimethyl ester[20] which was then saponified to afford the diacid coupling partner[21] (Figure 2b) for the on-resin dimerization among the N-deprotected terminal amines presented on the synthesis support to provide the symmetric OPV2 (**2**).

The synthesis of the OPV3 π-conjugated subunits revealed solubility issues that initially motivated the development of the on-resin dimerization procedure. The OPV3 amino acid proved to be difficult to synthesize, with a successful route coming from the two-step sequential Heck coupling onto *p*-divinylbenzene (Figure 3a): the first with 4-iodoaniline and

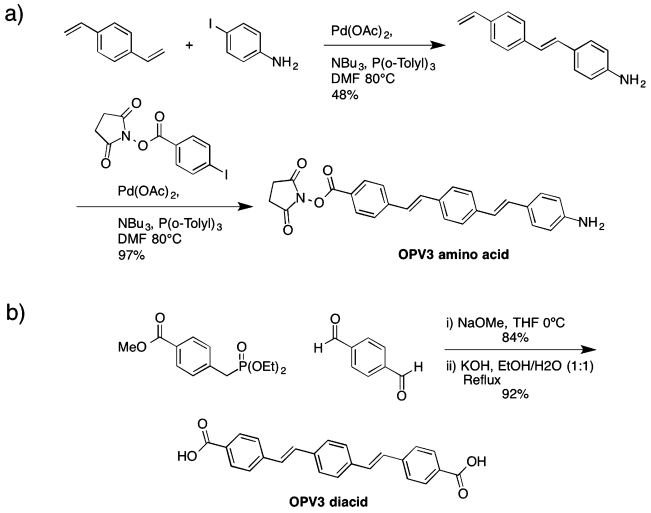

Figure 3. Synthesis of OPV3 amino acid (a) and diacid (b) for incorporation into nonsymmetric and symmetric peptide backbones present in **3** and **4**, respectively.

the second with the NHS-activated ester of 4-iodobenzoic acid. The sequential Heck reactions gave the isolable and directly acid-activated OPV3 amino acid that could be directly coupled onto the primary amine of the deprotected Wang resin without the need for aryl amine protection. This reduced nucleophilicity required that the subsequent amidation/N-acylation of the terminal aryl amine with Fmoc-glycine to continue the SPPS be conducted under the same electrophilic coupling conditions (triphosgene and 2,6-lutidine) as necessary for SPPS with the OPV2 amino acid, thus yielding the nonsymmetric OPV3 peptide (**3**). The symmetric OPV3 diacid was synthesized previously[16] through a double Horner−Wadsworth−Emmons reaction between terephthaldehyde and a benzylic phosphonate followed by subsequent saponification of the methyl esters[22] (Figure 3b). This diacid was used for the on-resin dimerization similarly to the OPV2 diacid, leading to the previously reported symmetric OPV3 peptide (**4**).

Model of Peptide Aggregation. The standard model invoked to understand the aggregation of these molecules is their self-assembly into extended β-sheet-like structures (Figure 4).[11−13] This picture is motivated by simplistic energy minimization calculations, which predict these ordered one-dimensional aggregates to be the most energetically favorable conformations at 0 K. Our more recent work employing molecular dynamics simulations at finite temperature has shown that entropic considerations are also important for a complete understanding of the thermodynamics and structure of these aggregates[15] and predict the perfect periodic order to

dx.doi.org/10.1021/la501999g | *Langmuir* 2014, 30, 11375−11385

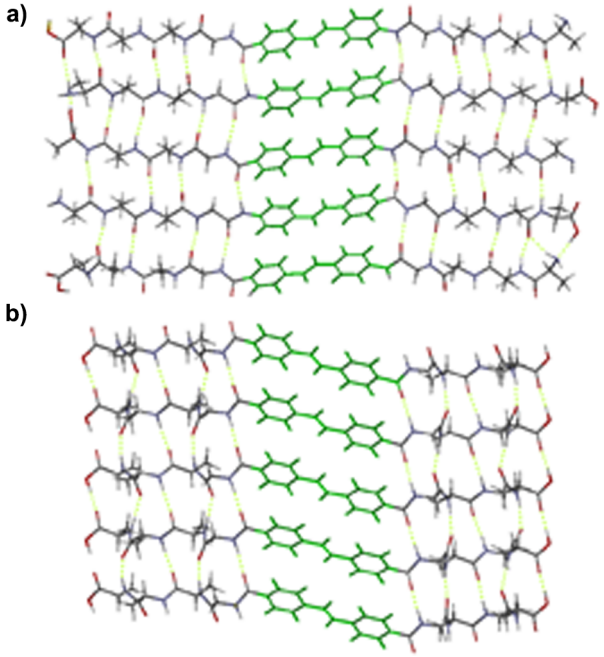

Figure 4. Energy-minimized models for the assembly of nonsymmetric (a) and symmetric (b) OPV2 oligopeptides, illustrating idealized antiparallel and parallel β-sheet structures, respectively. For simplicity, the aspartic acid and phenylalanine residues have been replaced with alanine.

break down, while still (and importantly) retaining one-dimensionality. While our experimental and computational results presented herein and elsewhere[15] paint a significantly more complex picture of assembly, the β-sheet-like structures presented in Figure 4 provide a useful pedagogical idealization for beginning to understand assembly and are broadly consistent with the observed morphological outcomes, electronic responses, and molecular simulations.

The symmetric (**2** and **4**) and nonsymmetric (**1** and **3**) peptide architectures synthesized in this work present an ideal starting point to understand how formal variations in the requisite hydrogen-bonding patterns possible within idealized nanostructures impact their photophysical properties. Our simple model would predict that the nonsymmetric peptides **1** and **3** would maximize favorable energetic interactions by assembling into 1-D aggregates consisting of antiparallel β-sheet motifs, whereas the architecture of the symmetric peptides **2** and **4** would constrain them to form less favorable parallel β-sheets. These assembled ribbons are presumed to aggregate into higher order structures (stacked fibrils, etc.) typical of oligopeptide and amyloid-like materials.[23] This simple modeling scenario places the π-conjugated units into distances close enough to expect electronic interactions and specific spectral signatures, and the computational and experimental studies we describe below provide strong support for the presence of these interactions. The designed symmetries of these molecules necessarily require phenylalanine steric clashing in both the parallel and antiparallel configurations. We have previously characterized these interactions for peptide **4** (symmetric OPV3)[15] and also observed polydiacetylene formation from assembled peptide−diacetylene−peptide precursors.[24] These findings are all consistent with sufficient local intermolecular ordering among the individual oligopeptides (and the reactive π-conjugated diyne subunits) to encourage electronic interactions and even covalent chemistry in a topochemical sense.

Nanostructure Morphology. The acidic residues effectively render all four peptides molecularly dissolved and not significantly interacting at basic pH (ca. pH 10). Acidification of the aqueous solutions (ca. pH 2) formally protonates the carboxylate groups and screens the Coulombic repulsions among the molecules, thereby allowing for intermolecular association and subsequent nanostructure formation. The OPV3 nanomaterials were found to bind Congo Red, thus revealing their amyloidogenic nature. Transmission electron microscopy (TEM) was employed to visualize the nanomaterials resulting from peptide assembly. It is well established that variations in peptide sequence can have dramatic morphological outcomes on molecular assembly, with structures spanning 0-D vesicles and micelles, 1-D tapes, rods, and ribbons, and 2-D sheet-like assemblies. When considering the photophysical properties inherent to such geometrically disparate objects, it is possible that local differences in packing densities, curvatures, etc., could influence the spectral outcomes regardless of specific structural variables. It was therefore important to find that the nanomaterials afforded by the assembly of symmetric and nonsymmetric peptides were comparable in their morphologies: all peptides examined yielded 1-D nanostructures with consistent widths (10−12 nm) as determined by TEM (Figure 5). Given that the molecular lengths of these peptides are well

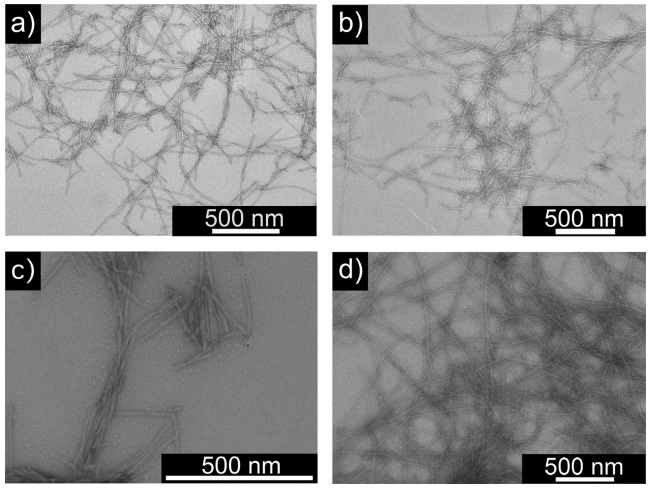

Figure 5. TEM micrographs of peptide nanostructures prepared from 0.1 wt % of the respective DFAG peptides in acidic solution along with their calculated widths: (a) nonsymmetric OPV3 (**3**: 9.6 ± 1.4 nm); (b) nonsymmetric OPV2 (**1**: 10.4 ± 1.6 nm); (c) symmetric OPV3 (**4**: 10.5 ± 1.3 nm); (d) symmetric OPV2 (**2**: 11.6 ± 1.8 nm).

under 10 nm in their fully extended conformations, the present structures reflect the inherent hierarchical bundling known to be operative in peptide-based self-assembling materials but nevertheless all remain comparable in size and shape. In all cases, nanostructures with high aspect ratios were observed, typically extending to micron lengths. These nanostructures can be viewed as experimental manifestations of the idealized assemblies shown in Figure 4 once extended along the π-stacking axis.

Photophysical Characterization. The assembly of these triblock molecules offers several possible intermolecular electronic outcomes that have distinct spectral observables. For example, exciton coupling via a classic H-like aggregate

dx.doi.org/10.1021/la501999g | *Langmuir* 2014, 30, 11375−11385

would lead to a blue-shift in the absorption maxima relative to the isolated molecules, a quenched photoluminescence, and, given the chirality expected for natural peptide aggregates, an induced CD signal and bisignate Cotton effect corresponding to the $\pi-\pi^*$ transition the OPV subunit. These general trends have been observed in similar peptide-π-peptide motifs.[11,13,16] Other possibilities include aggregates that may place the π-electron units into J-like aggregates that would lead to red-shifted absorption maxima and oftentimes enhanced photoluminescence or aggregated states with differing degrees of chromophore planarity/rigidity that otherwise do not exhibit any noticeable intermolecular electronic interactions. Given the differences in hydrogen-bonding networks expected to exist within nanostructures formed from the symmetric and nonsymmetric peptide frameworks, a careful spectroscopic explication of these electronic properties is warranted. The polydispersities in nanomaterial morphologies indicate that the spectral measurements should be treated as ensemble averages over all local chromophore orientations present rather than corresponding to a single defined orientation (such as within a crystalline lattice).

OPV2. Aggregated stilbene systems have typically shown two distinct spectral behaviors: one exhibiting broad featureless red-shifted emission typically accompanied by subtle changes in the absorption spectra and the other exhibiting structured emission profiles and perturbed absorption spectra compared to the isolated stilbene molecules. These two cases have been attributed to structural differences of the aggregate stilbenes with the first class corresponding to excimer-like emission appearing to have neighboring face-to-face interactions of the stilbene subunits and the second class corresponding to excitonic-like emission with edge-to-face interactions between the subunits.[25−27]

The nonsymmetric and symmetric OPV2 peptides **1** and **2** showed typical absorption and emission profiles in basic solution. Both peptides had identical absorption properties under both molecular and assembled conditions with λ_{max} values around 330 nm (Figure 6 and Table 1). The lack of apparent blue-shifts upon OPV2 assembly can be attributed to the shorter expected transition dipole (or the weaker oscillator strength of the $\pi-\pi^*$ transition) of these small chromophores that therefore do not experience as dramatic of an exciton coupling as in longer chromophores. The differences in PL between the two molecules can be rationalized by the different chemical compositions of the chromophores themselves (an *N*-acylcarboxamide and a dicarboxamide, respectively). Although the *N*-acyl nitrogen is likely participating in amide bond resonance, it is possible that it could serve as an electron donor for the accepting carboxamide on the other end of the chromophore unit. Once the pH of the spectroscopic solution was lowered (thus triggering the assembly), the absorption profiles did not change to any appreciable extent, but the photoluminescence was predominately excimeric in nature with featureless and broad peaks appearing at lower energies versus the respective monomers (λ_{max} differences of ca. 64 and 79 nm, Figure 6a,b). The PL red-shifts noted for the nonsymmetric peptides under both molecular and assembled conditions when compared to the symmetric could reflect a stronger "donor−acceptor" character that is better stabilized in the excited state. Remarkably, although the absolute values were low, there were no dramatic decreases in quantum yield upon assembly of either OPV2 examples; in fact, there was a notable increase in PL quantum yield for **1** upon assembly. The trends in excited

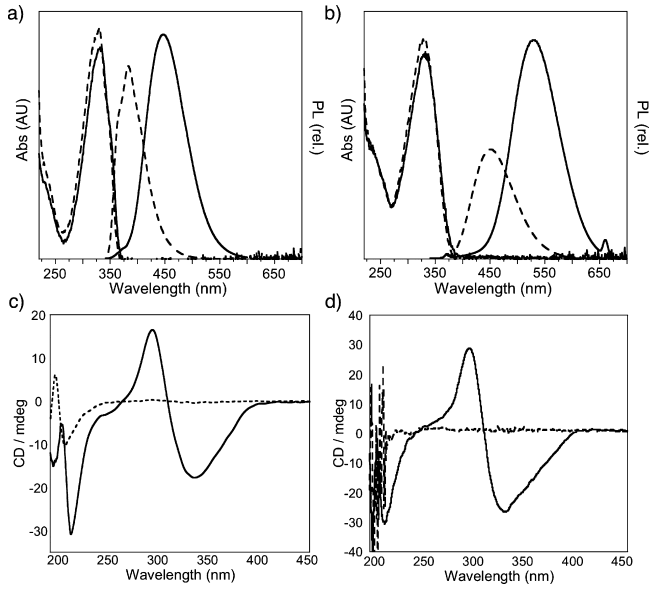

Figure 6. UV−vis and PL spectra (a, b) and CD spectra (c, d) of symmetric OPV2 (**2**: a, c) and nonsymmetric OPV2 (**1**: b, d) peptides in basic solution (- - -) and assembled in acidic solution (—).

state properties were comparable among the two examples: The single-exponential photoluminescence lifetimes recorded for the symmetric and nonsymmetric OPV 2s in basic solution were 0.31 and 0.23 ns, respectively, while extending to 0.74 and 0.99 ns, respectively, in acidic solution (Table 1). We observed that, under continual irradiation, basic molecular solutions and acidic aggregate solutions showed evidence for *trans−cis* isomerism, but we were unable to conclusively observe or otherwise characterize any significant contributions from intermolecular [2 + 2] stilbene photodimerizations as being facilitated by close contact within the assembled nanostructures (Figures S24 and S25).

Circular dichroism was used to interrogate the associations of the π-conjugated OPV chromophores before and after nanostructure assembly. Both OPV2 peptides showed no appreciable low-energy features in CD spectra for the basic molecularly dissolved samples, but upon lowing the pH to trigger the assemblies, bisignate spectral features crossing over around 310 nm were apparent (Figure 6c,d). The induction of such pronounced Cotton effects indicates that the stilbene moieties are held in chiral environments and, along with the excimeric-like emission profiles observed, that the stilbene subunits are in close contact as suggested by our modeling studies. Circular dichroism and infrared spectroscopies were also employed to ascertain information about the hydrogen-bonding networks. Both measurements indicated β-sheet-like character: CD revealed high-energy negative peaks at 205−210 nm along with classic IR amide I bands appearing at 1641 and 1632 cm^{-1} and amide II bands appearing at 1531 and 1537 cm^{-1} for the nonsymmetric and symmetric OPV2s, respectively. We emphasize that this data, recorded on lyophilized solid samples, does not allow us to specifically categorize the nature of the β-sheet character (specifically being parallel or antiparallel as idealized in Figure 4), nor does it rule out other more disordered peptide conformations. The intermolecular electronic interactions evident in the OPV2 signatures indicate that the π-electron portions are able to interact comparably

dx.doi.org/10.1021/la501999g | *Langmuir* 2014, 30, 11375−11385

Table 1. Steady-State and Time-Resolved Spectroscopic Data for the Peptide Variants

	Abs λ_{max}/nm		PL λ_{max}/nm[a]		QY[b]		τ/ns[c]	
peptide sequence	basic	acidic	basic	acidic	basic	acidic	basic	acidic
nsOPV2 (**1**)	330	330	451	530	0.02	0.04	0.23 (100)	0.99 (100)
sOPV2 (**2**)	330	334	383	447	0.06	0.06	0.31 (100)	0.74 (100)
nsOPV3 (**3**)	367	332	500	490	0.12	0.06	0.68 (100)	6.96 (28); 0.74 (72)
sOPV3 (**4**)	368	344	447	456	0.38	0.12	1.09 (100)	7.53 (100)

[a]Excitation at the absorption λ_{max}. [b]Recorded on solutions with absorbance below 0.1 au and relative to quinine sulfate in 0.5 N H_2SO_4 (0.55). [c]Fitted percent contributions for the decay profiles in parentheses.

within the nanostructures regardless of the specific hydrogen-bonding geometries being adopted within them.

The interpretation that the stilbene moieties undergo intermolecular electronic interactions is further corroborated by the excimer formation found in Letsinger's work with stilbene dicarboxamides placed into the backbones of complementary oligonucleotides.[28] These studies revealed only a minor (6 nm blue-shift) ground state perturbation upon hybridization (thus bringing the stilbene units sufficiently close for intermolecular electronic interactions) as well as a new fluorescent emission signature centered at 450 nm. Comparable results were found in Collard's work with cofacial stilbenes linked through a common [2.2]paracyclophane core that provides a more geometrically well-defined yet pre-existing ground-state through-space interaction.[29] Lewis' studies of arenedicarboxamide single crystals also provide insight into the effects of how torsional angles impact intermolecular interactions through specific perturbations arising from increased interplanar distances, lateral displacement, or twist angle with respect to adjacent monomers.[30] The peptide−OPV hybrids allow us to explore these effects with similar stilbene cores after the peptides assemble into nanostructures with comparably well-defined geometrical constraints.

OPV3. The distyrylbenzene chromophore is another well-defined OPV oligomer that has been subject to extensive photophysical study, similarly revealing a spectrum of electronic outcomes that varies as a function of intermolecular orientation. We previously interrogated a series of symmetric OPV3 peptides with systematic and site-specific variation of amino acid sequence and demonstrated the accessibility of excitonic and excimeric excited states.[15] In the present work, we challenge the central OPV3 chromophore with different peptide N-to-C directionalities of an otherwise constant amino acid sequence.

Both OPV3s have similar molecularly dissolved UV−vis absorption profiles (λ_{max} 367−368 nm) regardless of the chromophore connectivity (*N*-acylcarboxamide in **3** vs dicarboxamide in **4**) although the emission λ_{max} values were separated by ca. 50 nm (Figure 7 and Table 1). The OPV3 PL lifetimes for the molecularly dissolved solutions were 1.09 and 0.68 ns for the symmetric and nonsymmetric cases, respectively. Upon assembly, both OPV3 peptides showed the absorption trends typically associated with H-like aggregates: the UV−vis profiles showed an overall blue-shift in the absorption maxima with respect to the molecularly dissolved molecules (λ_{max} values of 332 and 343 nm for the nonsymmetric and symmetric OPV3s **3** and **4**, respectively) along with the appearance of weak lower energy shoulders at ca. 425 nm (Figure 7a,b). Unlike the OPV2 examples, the photoluminescence for both OPV3 aggregates was substantially quenched with respect to the isolated molecules (Figure 7c,d), and the lifetimes of the excited states were significantly

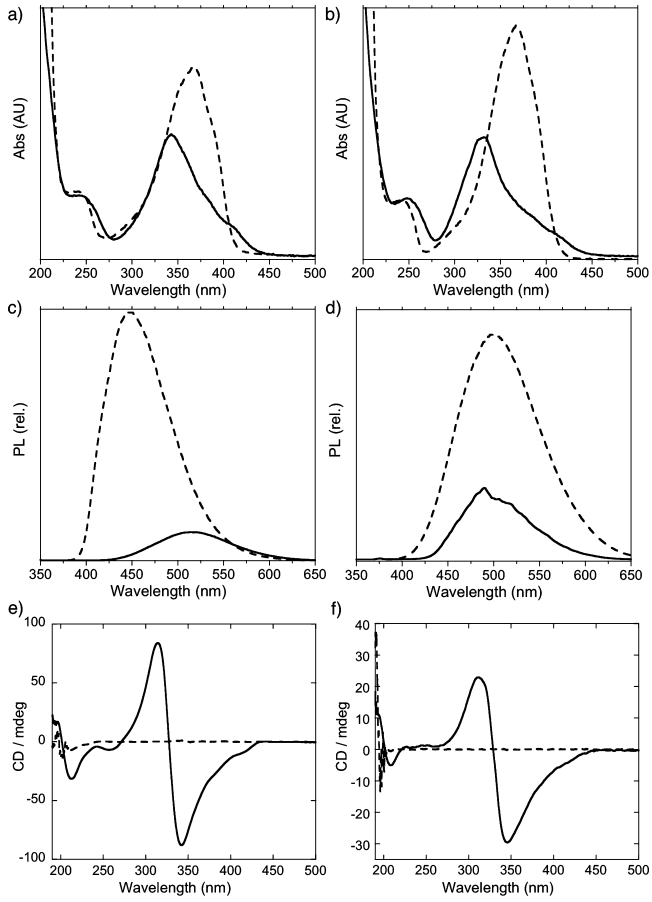

Figure 7. UV−vis (a, b), PL (c, d), and CD spectra (e, f) of symmetric OPV3 (**4**: a, c, e) and nonsymmetric OPV3 (**3**: b, d, f) peptides in basic solution (- - -) and assembled in acidic solution (—).

increased. This shows that the radiative and nonradiative rates of excited state decay are fundamentally different for these particular OPV2 and OPV3 chromophores under the conditions studied. Interestingly, the PL spectral footprints for the two OPV3 systems were markedly different. The PL of the symmetric OPV3 peptide **4** previously was shown to exhibit an excimeric structure with a red-shifted emission maxima centered at 515 nm with a single-component lifetime of 7.53 ns. In contrast, the nonsymmetric OPV3 peptide **3** had a spectral profile (evolution of vibronic fine structure but with no dramatic red-shift) and an excited-state lifetime (two components: 0.74 ns (72%) and 6.96 (28%)) more suggestive of the excitonic extreme. Polymodal PL signatures are characteristic of donor−acceptor types of OPV3 chromophores in exciton-coupled environments.[31,32] Although the assembled nonsymmetric OPV3 does not present clear vibronic features, it is much more structured than the broad and featureless

dx.doi.org/10.1021/la501999g | *Langmuir* 2014, 30, 11375−11385

spectrum recorded under molecular dissolution at basic pH. The absolute differences in PL maxima, as for the OPV2 cases, can be attributed to the donor−acceptor character present in the nonsymmetric OPV3 molecule. Although the two OPV3 chromophores are different, the greater contributions of the long-lived excited state component for symmetric OPV3s were previously correlated to the excimeric states, while the assemblies with greater contributions of shorter lived components were attributed to exciton-coupled states.

The circular dichroism spectra of the two OPV3 peptides were similar, with a negative Cotton effect showing a crossover point at ca. 330 nm. Furthermore, both OPV3 peptides showed negative signals centered at ca. 210 nm accompanied by IR signatures characteristic of amide I stretches (1635 and 1640 cm^{-1} for the symmetric and nonsymmetric, respectively) and amide II stretches (1535 and 1517/1531 cm^{-1}, respectively). As was the case for the OPV2 comparison, we are unable to extract definitive peptide hydrogen-bonding content out of these data. The split couplets in the low-energy portion of the CD spectra coupled with the UV−vis and PL data support the presence of exciton coupling among the longer OPV3 chromophores regardless of peptide sequence directionality or inherent conformational preferences.

Molecular Dynamics Simulations. The origin of the differences in excited state outcomes for the OPV2 peptides (both excimeric in nature) and the OPV3 peptides (one excimeric and one excitonic) were not immediately clear after considering intermolecular associations in energy-minimized models. We therefore turned to molecular dynamics simulations which present a means to furnish microscopic understanding of the interactions and thermodynamic driving forces driving assembly at a resolution inaccessible by experimentation. Because the first step in the self-assembly of nascent 1-D peptide ribbons is the formation of noncovalent peptide homodimers, we performed atomistic molecular dynamics simulations to model dimerization for each of the four DFAG peptides in Figure 1 (rather than model extended oligomeric stacks) to compute the free energy of dimerization, identify stabilizing interactions within the dimer, and test our hypothesis that the nonsymmetric peptides should preferentially adopt an antiparallel, rather than parallel, β-sheet motif. This dimeric restriction offers a more quantitative local picture about dimer geometries and energetics that should reasonably propagate within an extended supramolecular stack but with less computational demand. Details of our simulation protocols are provided in the Experimental Section.

Free Energy of Dimerization and Dimer Structure. To evaluate the free energy of dimerization, we computed from our simulations the Gibbs free energy—commonly referred to as the potential of mean force (PMF)—as a function of the distance between the molecular centers of mass, $G(\Delta r) = -k_B T \ln P(\Delta r) + C$, where k_B is Boltzmann's constant, T is the temperature, $P(\Delta r)$ is the equilibrium probability of observing the molecules at intermolecular center of mass distance Δr, and C is an additive constant due to the unknown normalization factor for the probability distribution (i.e., the partition function). Because of this additive constant, only differences in $G(\Delta r)$ are meaningful. The negative gradient of the PMF may be identified as an effective driving force along Δr averaged over the ensemble of system configurations at the corresponding value of Δr,[33] and the global minimum of the PMF corresponds to the most probable intermolecular separation at equilibrium. For the nonsymmetric peptide variants, we simulated the formation of both the parallel (i.e., molecules possess the same N-terminal to C-terminal directionality; parallel β-sheet motif) and antiparallel (i.e., peptides possess opposing N-terminal to C-terminal directionality; antiparallel β-sheet motif) dimers. In Figure 8, we present our computed

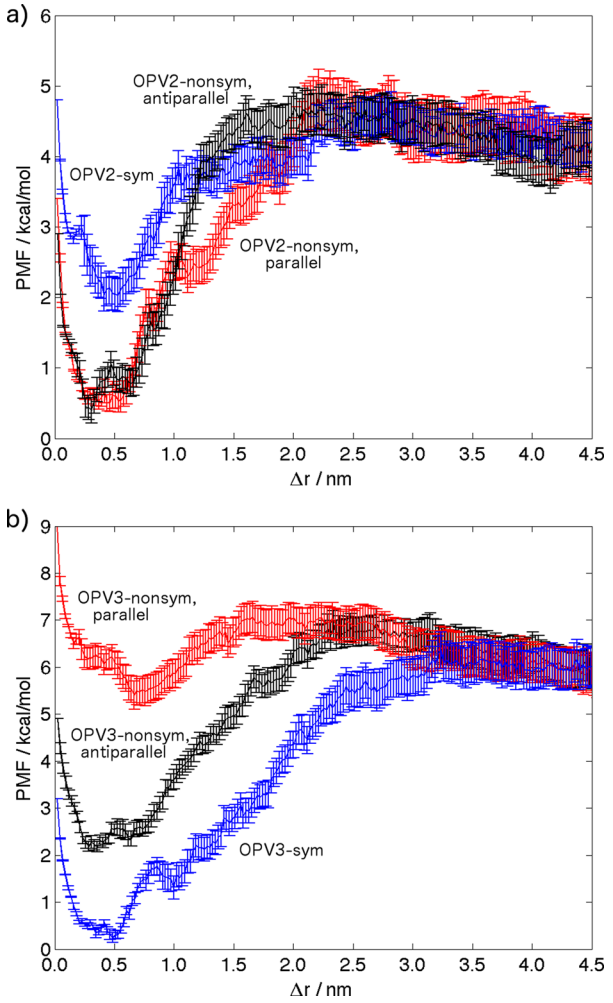

Figure 8. PMF profiles for the formation of peptide homodimers as a function of peptide center of mass distance, Δr, for symmetric and nonsymmetric (a) OPV2 and (b) OPV3 peptides.

PMF profiles for dimerization of the OPV2 and OPV3 peptides, and Figure S23 presents representative snapshots of dimer configurations generated using VMD.[34]

At large intermolecular distances, interactions between the molecules are screened by the intervening solvent, and the molecules are effectively noninteracting, reflected in the plateau in the PMF profiles at large separations, where the free energy ceases to be a function of separation. Consistent with the expectation that dimerization should proceed spontaneously, the PMF decreases as the intermolecular separation is reduced until it reaches a global minimum corresponding to the most probable intermolecular separation of the dimer contact pair. For all six systems considered, the PMF minimum lies in the range 0.3−0.7 nm, consistent with the expected model of aggregate formation in which the molecules mimic the assembly of natural peptides into β-sheet motifs that possess interstrand distances of about 0.5 nm.[26,35]

dx.doi.org/10.1021/la501999g | *Langmuir* 2014, 30, 11375−11385

The free energy change upon dimerization of the OPV2 peptides is about −2.2 kcal/mol for the symmetric architecture (**2**) and −3.7 kcal/mol for the nonsymmetric architecture (**1**). The PMF profile for the symmetric dimer possesses a minimum at 0.53 ± 0.06 nm, whereas those for the parallel and antiparallel nonsymmetric homodimers exhibit minima at intermolecular separations of 0.44 ± 0.06 and 0.31 ± 0.06 nm, respectively. There is no statistically significant difference in the dimerization free energy change for the parallel and antiparallel nonsymmetric dimer pairs. The absence of a strong thermodynamic orientational preference suggests that multimeric 1D aggregates of nonsymmetric OPV2 peptides may contain a statistical mixture of idealized parallel and antiparallel β-sheet motifs. Thus, there is a strong statistical overlap in the intermolecular spacings for both OPV2 molecules that can serve to rationalize the similarities in excited state excimeric outcomes regardless of peptide directionality or hydrogen-bonding networks present within the resulting nanostructures.

For the OPV3 peptides, the free energy change upon dimerization for the symmetric architecture (**4**) is about −5.8 kcal/mol, and the intermolecular separation at the PMF minimum is 0.48 ± 0.06 nm. This separation is statistically consistent with the spacing found for this peptide as part of a 35-membered stack reported previously (DFAG).[15] For the nonsymmetric OPV3 peptides (**3**), the free energy change for formation of the antiparallel homodimer is about −3.7 kcal/mol, compared to only −0.6 kcal/mol for the parallel orientation. The intermolecular separation in the antiparallel homodimer is 0.36 ± 0.06 nm, compared to 0.67 ± 0.06 nm for the less stable parallel orientation. This suggests that 1D aggregates of nonsymmetric OPV3 peptides possess an intrinsic bias toward the more stable antiparallel peptide orientations that resemble antiparallel β-sheet motifs. The essentially complete lack of intermolecular stacking overlap among the likely configurations of the two OPV3 configurations could help to rationalize the different excited state outcomes observed. Consistent with our prior sequence variation analysis,[15] aggregates with smaller intermolecular spacings tended toward excitonic states whereas larger spacings coincided with excimeric states.

We summarize in Table 2 the intermolecular separation, Δr_{dimer}, and relative twist angle between the peptides, $\Delta\theta_{dimer}$, in the dimer and the free energy change for dimerization, $\Delta G_{dimerization}$, for each of the six configurations. The relative twist angle between the molecules in the OPV2 dimers averaged over the configurational ensemble observed in our simulations is not statistically significantly different from zero, suggesting that the molecules—at least in the dimer—show little preference to deviate from a near parallel stacking configuration. In contrast, the OPV3 dimers all possess nonzero twist angles within the standard deviation of the ensemble, suggesting an intrinsic preference for a skewed stacking configuration (cf. Figure S23).

Table 2. Free Energy Change, Intermolecular Separation, and Relative Twist Angle between Molecules in the Dimer

dimer[a]	orientation	$\Delta G_{dimerization}$[b] (kcal/mol)	Δr_{dimer}[c] (nm)	$\Delta\theta_{dimer}$[d] (deg)
s OPV2 (**2**)		−2.2 ± 0.4	0.53 ± 0.06	4 ± 14
ns OPV2 (**1**)	parallel	−3.6 ± 0.4	0.44 ± 0.06	6 ± 15
ns OPV2 (**1**)	antiparallel	−3.8 ± 0.4	0.31 ± 0.06	12 ± 8
s OPV3 (**4**)		−5.8 ± 0.4	0.48 ± 0.06	8 ± 6
ns OPV3 (**3**)	parallel	−0.6 ± 0.5	0.67 ± 0.06	11 ± 6
ns OPV3 (**3**)	antiparallel	−3.7 ± 0.4	0.36 ± 0.06	22 ± 9

[a]s = symmetric, ns = nonsymmetric. [b]Uncertainties computed by 50 rounds of bootstrap resampling and propagation of uncertainties. [c]Uncertainties from bin resolution of calculated PMF curve. [d]Standard deviation computed over all umbrella sampling configurations satisfying $\Delta r = \Delta r_{dimer} \pm 0.06$ nm. Since the peptides in the homodimer are identical, we have adopted a convention in which the relative angle is taken to be non-negative.

Energetics of Dimerization. Consistent with our molecular model of self-assembly of peptides into 1-D aggregates consisting of β-sheet-like motifs, it was our anticipation that the stability differences between the various homodimers may be explained by the efficiency of hydrogen bonding within the dimer. We report in Table 3 the number of intermolecular hydrogen bonds formed between the peptides in each of the six homodimers. The similar stability of the parallel and antiparallel nonsymmetric OPV2 dimers is consistent with the formation in each case of around two interpeptide hydrogen bonds. The elevated stability of the antiparallel OPV3 dimer over the parallel configuration is consistent with the formation of approximately one extra hydrogen bond in the antiparallel orientation. Because of the polydisperse nature of the assembled structures that form, we are unable to definitively correlate these energetics to specific assembly morphologies (e.g., those shown in Figure 5). Future work will seek to further understand the energetics of the longer range assembly processes operative in these nanomaterials.

The relative stabilities of the symmetric and nonsymmetric dimers cannot be rationalized by hydrogen bonding alone, so to more quantitatively probe the energetics of dimerization, we decomposed the total system interaction energy to compute: (i) $\Delta U_{peptide}$ as the portion of the energy change resulting from bonded interactions (bonds, angles, dihedrals) and intramolecular nonbonded contributions (van der Waals, Coulomb) within both peptides upon dimerization and (ii) $\Delta U^{vdW}_{peptide-peptide}$ and $\Delta U^{Coul}_{peptide-peptide}$ as the changes in the intermolecular van der Waals and Coulomb interactions between the molecules upon formation of the dimer. We summarize these energy changes upon dimerization in Table 3. Negative terms correspond to energetic contributions that favor dimerization. For all systems studied, the change in intramolecular peptide energies upon dimerization cannot be distinguished from zero with the calculated standard deviations. This is consistent with our observation that peptide conformations change very little over the course of dimerization.

The aggregated van der Waals and Coulombic contributions to the peptide−peptide dimerization energy change, $\Delta U_{peptide-peptide} = \Delta U^{vdW}_{peptide-peptide} + \Delta U^{Coul}_{peptide-peptide}$, is significantly smaller for the formation of the parallel nonsymmetric OPV3 dimer (−34 kcal/mol) relative to both the antiparallel nonsymmetric (−46 kcal/mol) and symmetric (−45 kcal/mol) dimers. The more favorable Coulombic interactions in the antiparallel nonsymmetric dimer relative to the parallel orientation is consistent with a strong planar hydrogen bonding pattern in the idealized antiparallel β-sheet motif, compared to the weaker nonplanar pattern in the parallel arrangement. The values of $\Delta U_{peptide-peptide}$ for the antiparallel nonsymmetric and symmetric dimers are very similar, indicating that the ∼2 kcal/mol higher stability of the symmetric dimer cannot be explained by intermolecular interactions alone (cf. Table 2). In the case of OPV2, both the van der Waals and Coulombic contributions to $\Delta U_{peptide-peptide}$ are substantially larger for the antiparallel

dx.doi.org/10.1021/la501999g | Langmuir 2014, 30, 11375−11385

Table 3. Hydrogen Bonds Formed and Decomposition of the Energy Change upon Dimerization

dimer[a]	orientation	no. H-bonds[b]	$\Delta U_{peptide}$[b] (kcal/mol)	$\Delta U^{vdW}_{peptide-peptide}$[b] (kcal/mol)	$\Delta U^{Coul}_{peptide-peptide}$[b] (kcal/mol)	$\Delta U_{peptide-peptide}$[b] (kcal/mol)
s OPV2		2.0 ± 1.2	1 ± 29	−23 ± 4	−14 ± 8	−37 ± 9
ns OPV2	parallel	2.0 ± 1.3	−22 ± 34	−26 ± 4	−13 ± 6	−39 ± 7
ns OPV2	antiparallel	1.8 ± 1.0	−2 ± 31	−30 ± 5	−17 ± 5	−47 ± 7
s OPV3		2.3 ± 0.7	3 ± 29	−32 ± 3	−13 ± 4	−45 ± 5
ns OPV3	parallel	0.9 ± 0.9	10 ± 33	−27 ± 4	−7 ± 5	−34 ± 6
ns OPV3	antiparallel	2.3 ± 1.7	3 ± 39	−31 ± 5	−15 ± 12	−46 ± 13

[a]s = symmetric, ns = nonsymmetric. [b]Standard deviations computed over all umbrella sampling configurations satisfying $\Delta r = \Delta r_{dimer} \pm 0.06$ Å and propagation of uncertainties.

nonsymmetric OPV2 dimer relative to the symmetric orientation, again consistent with the elevated stability of the antiparallel β-sheet motif. Nevertheless, the free energy calculations (cf. Table 2) reveal the antiparallel dimer to be only ∼0.2 kcal/mol more stable than the parallel, despite possessing an approximately 8 kcal/mol more favorable peptide−peptide interaction energy.

The results of our energy analysis support our hypothesis that the antiparallel arrangement of nonsymmetric dimers should be energetically favored over the parallel arrangement due to more efficient intermolecular interactions. In all cases the van der Waals contribution to the peptide−peptide interaction outweighs the Coulomb, with dispersion interactions responsible for 62−79% of the total interaction energy, indicating an important role for nonspecific dispersion interactions in addition to specific hydrogen bonds. The free energy of dimerization comprises enthalpic and entropic contributions, $\Delta G_{dimerization} = \Delta H - T\Delta S$, which may be further decomposed as $\Delta G_{dimerization} = \Delta U_{peptide} + \Delta U_{peptide-peptide} + \Delta U_{peptide-solvent} + \Delta U_{solvent} + p\Delta V - T\Delta S$. We have quantified in the present study $\Delta G_{dimerization}$, $\Delta U_{peptide}$, and $\Delta U_{peptide-peptide}$. That the observed trends in $\Delta G_{dimerization}$ cannot be explained by the trends in $\Delta U_{peptide}$ and $\Delta U_{peptide-peptide}$ alone indicates that the peptide−solvent interaction, solvent energetics, and volumetric and entropic effects also make important contributions to the free energy of dimerization. While in principle this decomposition might be experimentally accessible from calorimetry,[36] these experiments would likely be exceedingly difficult to conduct in practice because controlling the formation of dimers without forming higher order aggregates would be extremely challenging. We are currently undertaking additional simulation studies to quantify the entropic and solvent-mediated enthalpic components of the calculated free energy of dimerization using the methodology detailed elsewhere.[37] Such calculations will furnish insight into the relative enthalpic and entropic contributions to the dimerization process and help guide the design of peptides engineered to stabilize and control aggregation.

CONCLUSIONS

We have reported a series of OPV-containing oligopeptides possessing similar primary amino acid sequences but differing in the presentation of overall peptide directionality. We explored the photophysical properties of their self-assembled nanostructures to probe how hydrogen-bonding networks would perturb the aggregate structure. Although the hydrogen-bonding motifs differ in their relative stability, the ability for each of these peptide constructs to self-assemble does not appear to be dramatically influenced. The OPV2 peptides seem to show nearly quantitative excimer emission regardless of peptide directionality, while the OPV3 peptides show a dichotomy in excited state outcome that depends on the nature of the hydrogen-bonding networks. This can be attributed in part to magnified differences in intermolecular spacing for the OPV3 peptides relative to the OPV2s. Molecular dynamics simulations for the formation of peptide homodimers as the first stage of peptide self-assembly reveal free energy changes driving dimerization of 2−6 kcal/mol. Intermolecular interactions between nonsymmetric OPV3 peptide pairs favor the formation of antiparallel dimers in a motif akin to an antiparallel β-sheet, contributing to the ∼3 kcal/mol enhanced stability of the antiparallel relative to the parallel orientation. In the case of the nonsymmetric OPV2 peptides, the antiparallel and parallel dimers are equally stable despite a ∼8 kcal/mol larger intermolecular interaction energy in the antiparallel orientation. These findings suggest an important role for solvent-mediated interactions and entropic effects in determining dimer stability. The geometric relationships within the dimer pairs provide a useful starting point for electronic structure calculations of the expected photophysical outcomes that will be the subject of future investigations. Potential results that come as a result of the hydrogen-bonding motif could help shed information about naturally occurring peptide aggregation as well as potential supramolecular materials, and differences that arise from this and the differing π-conjugated subunit can aid in understanding interchain interactions of extended π-conjugated systems that may more useful for exploring the bioelectronics potential of these materials.

EXPERIMENTAL SECTION

Specific details about the synthesis of π-conjugated amino acids, diacids, and peptide target molecules along with relevant characterization data for all synthetic intermediates and final peptide molecules may be found in the Supporting Information.

General Synthesis of Peptides. All peptides were synthesized using standard solid phase 9-fluorenylmethoxycarbonyl (Fmoc) chemistry on a Wang resin preloaded (0.8 mmol/g) with the Fmoc-protected Asp(O^tBu). Fmoc deprotection was performed by mixing the resin in a piperidine/DMF (2:8) solution for 10 min (2×), followed by rinsing with DMF, MeOH, and CH_2Cl_2. For all standard amino acid couplings, 3.0 equiv (relative to the resin substitution) of Fmoc protected amino acid was activated externally with 2.9 equiv of HBTU and 10 equiv of diisopropylethylamine (DIPEA) dissolved in NMP. The activated Fmoc-protected amino acid was then added to a peptide chamber containing the deprotected Wang resin and mixed for 3 h. The resin was then drained, rinsed with NMP, MeOH, and CH_2Cl_2, and then allowed to dry. All coupling and deprotection steps were monitored by performing a Kaiser test.

Installation of π-Conjugated "Amino Acids" (for Nonsymmetric Peptides 1 and 3). The Fmoc-protected OPV amino acids were coupled to immobilized and deprotected DFAG tetrapeptide sequences prepared as above but were activated with HATU rather then HBTU and a solution of 2:1 NMP/DCM was used

dx.doi.org/10.1021/la501999g | Langmuir 2014, 30, 11375−11385

for the couplings. After successful coupling and Fmoc deprotection as described above, the next Fmoc-protected α-amino acid residue (glycine) was activated with triphosgene and 2,4,6-trimethylpyridine using a published procedure.[6] At this point, standard SPPS was carried out as described above to install the remainder of the peptide sequence (A, F, and D amino acids).

Installation of π-Conjugated Diacids (for Symmetric Peptides 2 and 4). The general on-resin dimerization procedure of Vadehra et al. was followed for OPV2 diacid installation,[11] while the symmetric OPV3 was prepared similarly and as reported previously. 4,4′-((1*E*,1′*E*)-1,4-Phenylenebis(ethene-2,1-diyl))dibenzoic acid (0.3 equiv) and PyBOP (0.6 equiv) were dissolved in 2:1 NMP:CH_2Cl_2. DIPEA (7.0 equiv) was added and mixed for approximately 1 min. This solution was then added to the deprotected Wang resin with immobilized DFAG tetrapeptide (1.0 equiv) in a peptide chamber, and the reaction was mixed for 18 h. The chamber was drained, and the resin was washed with CH_2Cl_2, MeOH, and NMP. A second round of coupling was then performed: 4,4′-((1*E*,1′*E*)-1,4-phenylenebis-(ethene-2,1-diyl))dibenzoic acid (0.2 equiv) and PyBOP (0.4 equiv) were dissolved in 2:1 NMP:CH_2Cl_2. DIPEA (7.0 equiv) was added and mixed for approximately 1 min. The solution was then added to deprotected Wang resin (1.0 equiv) in a peptide chamber, and the reaction was mixed for 18 h. The chamber was drained, and the resin was washed with CH_2Cl_2, MeOH, and NMP.

General Procedure for Peptide Cleavage from the Resin. A 2:1 solution of 9.5:0.25:0.25 trifluoroacetic acid/H_2O/triisopropylsilane and CH_2Cl_2 were added to the peptide chamber and mixed with the resin for 3 h. The resin was removed by filtration and washed 3× with DCM, and the filtrate was then concentrated via solvent evaporation under reduced pressure. Cold Et_2O was added to the solution, and the resulting solid material was collected via centrifugation. After decanting the Et_2O, the crude material was dissolved in water, and ammonium hydroxide was added until the material was completely dissolved. This solution was lyophilized, and the obtained crude dry material was purified via reverse phase high performance liquid chromatography (RP-HPLC).

UV−vis and Photoluminescence. UV−vis spectra were collected using a Varian Cary 50 Bio UV−vis spectrophotometer. PL data were collected using a PTI Photon Technology International QuantaMaster Fluorometer with an Ushio xenon short arc lamp. Lifetime measurements were collected on the QuantaMaster fluorometer with a PTI TimeMaster LED TM-200 strobe. PTI FeliX32 V.1.2 (Build 56) was used for data processing. Micromolar samples were prepared using Millipore water, and the pH was adjusted by the addition of 1000 mL (for **1** and **2**) or 10 μL (for **3** and **4**) of 1 M HCl or 1 M KOH.

Circular Dichroism. CD spectra were acquired using a Jasco J-810 spectropolarimeter. Acidic and basic samples were prepared by adding 10 μL of 1 M HCl or 1 M KOH, respectively, to micromolar stock solution of the peptide in Millipore water.

Attenuated Total Reflection Infrared Spectroscopy. Data were obtained on dry lyophilized peptides using a Thermo Nicolet NEXUS 670 FTIR.

Transmission Electron Microscopy. TEM images were acquired on a Philips EM 420 transmission electron microscope equipped with an SIS Megaview III CCD digital camera. 300 mesh Formvar carbon coated copper grids were purchased from Electron Microscopy Sciences. Grids were prepared as follows: A stock solution of a 0.1 mg/mL peptide in Millipore water was exposed to concentrated HCl vapor for 1 min. 10 μL of this solution was pipetted onto a grid. The grid was incubated for 8 min. The grid was then dipped sequentially into water and then into a solution of 2% uranyl acetate stain and allowed to dry in air. ImageJ 1.47 (National Institutes of Health, Bethesda, MD) was used to approximate the widths and associated standard deviations of the nanostructures (n = 50 per TEM image).

Molecular Dynamics Simulations. Molecular dynamics simulations were conducted using the GROMACS 4.6 simulation suite.[38] Peptides were modeled using the CHARM27 force field,[39] and water was modeled explicitly using the TIP3P model.[40] Umbrella sampling[41] was employed to simulate dimerization by restraining the intermolecular distance between the peptide centers of mass and the free energy profile computed by solving the WHAM equations.[42] Full details of our simulation protocols are provided in the Supporting Information.

■ ASSOCIATED CONTENT

Supporting Information

General synthesis details, molecular characterization data, full details of the molecular simulations, and Figures S1−S25. This material is available free of charge via the Internet at http://pubs.acs.org.

■ AUTHOR INFORMATION

Corresponding Author

*E-mail: tovar@jhu.edu (J.D.T.).

Notes

The authors declare no competing financial interest.

■ ACKNOWLEDGMENTS

We thank Johns Hopkins University and the U.S. Department of Energy Office of Basic Energy Sciences (DE-SC0004857, J.D.T. and A.L.F. peptide nanomaterial synthesis and simulation) for financial support. We thank the Fairbrother group at JHU for assistance with ATR-IR measurements. B.D.W. was supported by the Harry and Cleio Greer Fellowship (JHU).

■ REFERENCES

(1) Caplan, M. R.; Lauffenburger, D. A. Nature's complex copolymers: Engineering design of oligopeptide materials. *Ind. Eng. Chem. Res.* **2002**, *41*, 403−412.

(2) Holmes, T. C. Novel peptide-based biomaterial scaffolds for tissue engineering. *Trends Biotechnol.* **2002**, *20*, 16−21.

(3) Ulijn, R. V.; Smith, A. M. Designing peptide based nanomaterials. *Chem. Soc. Rev.* **2008**, *37*, 664−675.

(4) Zelzer, M.; Ulijn, R. V. Next-generation peptide nanomaterials: molecular networks, interfaces and supramolecular functionality. *Chem. Soc. Rev.* **2010**, *39*, 3351−3357.

(5) Engler, A. J.; Sen, S.; Sweeney, H. L.; Discher, D. E. Matrix elasticity directs stem cell lineage specification. *Cell* **2006**, *126*, 677−689.

(6) Jatsch, A.; Schillinger, E. K.; Schmid, S.; Bäuerle, P. Biomolecule assisted self-assembly of π-conjugated oligomers. *J. Mater. Chem.* **2010**, *20*, 3563−3578.

(7) Gonzalez-Rodriguez, D.; Schenning, A. P. H. J. Hydrogen-bonded supramolecular π-functional materials. *Chem. Mater.* **2011**, *23*, 310−325.

(8) Kim, S. H.; Parquette, J. R. A model for the controlled assembly of semiconductor peptides. *Nanoscale* **2012**, *4*, 6940−6947.

(9) Marty, R.; Szilluweit, R.; Sanchez-Ferrer, A.; Bolisetty, S.; Adamcik, J.; Mezzenga, R.; Spitzner, E.-C.; Feifer, M.; Steinmann, S. N.; Corminboeuf, C.; Frauenrath, H. Hierarchically structured microfibers of "single stack" perylene bisimide and quaterthiophene nanowires. *ACS Nano* **2013**, *7*, 8498−8508.

(10) Tovar, J. D. Supramolecular construction of optoelectronic biomaterials. *Acc. Chem. Res.* **2013**, *46*, 1527−1537.

(11) Diegelmann, S. R.; Gorham, J. M.; Tovar, J. D. One-dimensional optoelectronic nanostructures derived from the aqueous self-assembly of π-conjugated oligopeptides. *J. Am. Chem. Soc.* **2008**, *130*, 13840−13841.

(12) Schillinger, E.-K.; Mena-Osteritz, E.; Hentschel, J.; Börner, H. G.; Bäuerle, P. Oligothiophene versus β-sheet peptide: Synthesis and self-assembly of an organic semiconductor-peptide hybrid. *Adv. Mater.* **2009**, *21*, 1562−1567.

(13) Stone, D. A.; Hsu, L.; Stupp, S. I. Self-assembling quinquethiophene-oligopeptide hydrogelators. *Soft Matter* **2009**, *5*, 1990−1993.

(14) Mba, M.; Moretto, A.; Armelao, L.; Crisma, M.; Toniolo, C.; Maggini, M. Synthesis and self-assembly of oligo(p-phenylenevinylene) peptide conjugates in water. *Chem.—Eur. J.* **2011**, *17*, 2044−2047.
(15) Wall, B. D.; Zacca, A. E.; Sanders, A. M.; Wilson, W. L.; Ferguson, A. L.; Tovar, J. D. Supramolecular polymorphism: Tunable electronic interactions within pi-conjugated peptide nanostructures dictated by primary amino acid sequence. *Langmuir* **2014**, *30*, 5946−5956.
(16) Vadehra, G. S.; Wall, B. D.; Diegelmann, S. R.; Tovar, J. D. On-resin dimerization incorporates a diverse array of π-conjugated functionality within aqueous self-assembling peptide backbones. *Chem. Commun.* **2010**, *46*, 3947−3949.
(17) Anthony, N. G.; Breerl, D.; Clarke, J.; Donoghue, G.; Drummond, A. J.; Ellis, E. M.; Gemmell, C. G.; Helesbeux, J.-J.; Hunter, I. S.; Khalaft, A. I.; Mackay, S. P.; Parkinson, J. A.; Suckling, C. J.; Waiah, R. D. Antimicrobial lexitropsins containing amide, amidine, and alkene linking groups. *J. Med. Chem.* **2007**, *50*, 6116−6125.
(18) Durantini, E. N. Synthesis of functional olefins using the Wittig-Horner reaction in different media. *Synth. Commun.* **1999**, *29*, 4201−4222.
(19) Falb, E.; Yechezkel, T.; Salitra, Y.; Gilon, C. In situ generation of Fmoc-amino acid chlorides using bis(trichloromethyl) carbonate and its utilization for difficult couplings in solid-phase peptide synthesis. *J. Pept. Res.* **1999**, *53*, 507−517.
(20) Eastoe, J.; Dominguez, M. S.; Wyatt, P.; Beeby, A.; Heenan, R. K. Properties of a stilbene-containing gemini photosurfactant: Light-triggered changes in surface tension and aggregation. *Langmuir* **2002**, *18*, 7837−7844.
(21) Gourianov, N.; Kluger, R. Conjoined hemoglobins. Loss of cooperativity and protein-protein lnteractions. *Biochemistry* **2005**, *44*, 14989−14999.
(22) Sancho-Garcia, J. C.; Bredas, J. L.; Beljonne, D.; Cornil, J.; Martinez-Alvarez, R.; Hanack, M.; Poulsen, L.; Gierschner, J.; Mack, H. G.; Egelhaaf, H. J.; Oelkrug, D. Design of π-conjugated organic materials for one-dimensional energy transport in nanochannels. *J. Phys. Chem. B* **2005**, *109*, 4872−4880.
(23) Davies, R. P. W.; Aggeli, A.; Beevers, A. J.; Boden, N.; Carrick, L. M.; Fishwick, C. W. G.; McLeish, T. C. B.; Nyrkova, I.; Semenov, A. N. Self-assembling β-sheet tape forming peptides. *Supramol. Chem.* **2006**, *18*, 435−443.
(24) Diegelmann, S. R.; Hartman, N.; Markovic, N.; Tovar, J. D. Synthesis and alignment of discrete polydiacetylene-peptide nanostructures. *J. Am. Chem. Soc.* **2012**, *134*, 2028−2031.
(25) Whitten, D. G. Photochemistry and photophysics of trans-stilbene and related alkenes in surfactant assemblies. *Acc. Chem. Res.* **1993**, *26*, 502−509.
(26) Lewis, F. D.; Yang, J. S.; Stern, C. L. Ground and excited-state aromatic-aromatic interactions with distance control by hydrogen-bonding. *J. Am. Chem. Soc.* **1996**, *118*, 2772−2773.
(27) Catalán, J.; Zimányi, L.; Saltiel, J. Medium-controlled aggregation of trans-stilbene. *J. Am. Chem. Soc.* **2000**, *122*, 2377−2378.
(28) Letsinger, R. L.; Wu, T. Control of excimer emission and photochemistry of stilbene units by oligonucleotide hybridization. *J. Am. Chem. Soc.* **1994**, *116*, 811−812.
(29) Mukhopadhyay, S.; Jagtap, S. P.; Coropceanu, V.; Brédas, J. L.; Collard, D. M. π-Stacked oligo(phenylene vinylene)s based on pseudo-geminal substituted [2.2]paracyclophanes: Impact of interchain geometry and interactions on the electronic properties. *Angew. Chem., Int. Ed.* **2012**, *51*, 11629−11632.
(30) Lewis, F. D.; Yang, J. S.; Stern, C. L. Crystal structures of secondary arenedicarboxamides. An investigation of arene-hydrogen bonding relationships in the solid state. *J. Am. Chem. Soc.* **1996**, *118*, 12029−12037.
(31) Bartholomew, G. P.; Bazan, G. C. Synthesis, characterization, and spectroscopy of 4,7,12,15-[2.2]paracyclophane containing donor and acceptor groups: Impact of substitution patterns on through-space charge transfer. *J. Am. Chem. Soc.* **2002**, *124*, 5183−5196.
(32) Hoeben, F. J. M.; Herz, L. M.; Daniel, C.; Jonkheijm, P.; Schenning, A. P. H. J.; Silva, C.; Meskers, S. C. J.; Beljonne, D.; Phillips, R. T.; Friend, R. H.; Meijer, E. W. Efficient energy transfer in mixed columnar stacks of hydrogen-bonded oligo(p-phenylene vinylene)s in solution. *Angew. Chem., Int. Ed.* **2004**, *43*, 1976−1979.
(33) Yu, T.; Lee, O.-S.; Schatz, G. C. Steered molecular dynamics studies of the potential of mean force for peptide amphiphile self-assembly into cylindrical nanofibers. *J. Phys. Chem. A* **2013**, *117*, 7453−7460.
(34) Humphrey, W.; Dalke, A.; Schulten, K. VMD: Visual molecular dynamics. *J. Mol. Graphics* **1996**, *14*, 33−38.
(35) Hughes, A. B. *Amino Acids, Peptides and Proteins in Organic Chemistry, Protection Reactions, Medicinal Chemistry, Combinatorial Synthesis*; Wiley-VCH: New York, 2011.
(36) Leavitt, S.; Freire, E. Direct measurement of protein binding energetics by isothermal titration calorimetry. *Curr. Opin. Struct. Biol.* **2001**, *11*, 560−566.
(37) Choudhury, N.; Pettitt, B. M. Enthalpy-entropy contributions to the potential of mean force of nanoscopic hydrophobic solutes. *J. Phys. Chem. B* **2006**, *110*, 8459−8463.
(38) Hess, B.; Kutzner, C.; van der Spoel, D.; Lindahl, E. GROMACS 4: Algorithms for highly efficient, load-balanced, and scalable molecular simulation. *J. Chem. Theory Comput.* **2008**, *4*, 435−447.
(39) MacKerell, A. D.; Bashford, D.; Bellott, M.; Dunbrack, R. L.; Evanseck, J. D.; Field, M. J.; Fischer, S.; Gao, J.; Guo, H.; Ha, S.; Joseph-McCarthy, D.; Kuchnir, L.; Kuczera, K.; Lau, F. T. K.; Mattos, C.; Michnick, S.; Ngo, T.; Nguyen, D. T.; Prodhom, B.; Reiher, W. E.; Roux, B.; Schlenkrich, M.; Smith, J. C.; Stote, R.; Straub, J.; Watanabe, M.; Wiorkiewicz-Kuczera, J.; Yin, D.; Karplus, M. All-atom empirical potential for molecular modeling and dynamics studies of proteins. *J. Phys. Chem. B* **1998**, *102*, 3586−3616.
(40) Jorgensen, W. L.; Chandrasekhar, J.; Madura, J. D.; Impey, R. W.; Klein, M. L. Comparison of simple potential functions for simulating liquid water. *J. Chem. Phys.* **1983**, *79*, 926−935.
(41) Torrie, G. M.; Valleau, J. P. Non-physical sampling distributions in Monte Carlo free-energy estimation - umbrella sampling. *J. Comput. Phys.* **1977**, *23*, 187−199.
(42) Roux, B. The calculation of the potential of mean force using computer-simulations. *Comput. Phys. Commun.* **1995**, *91*, 275−282.